Composites: Part A 149 (2021) 106530

Contents lists available at ScienceDirect

Composites Part A

journal homepage: www.elsevier.com/locate/compositesa

Bio-inspired adhesive joint with improved interlaminar fracture toughness

A. Wagih, R. Tao, G. Lubineau *

King Abdullah University of Science and Technology (KAUST), Physical Science and Engineering Division, COHMAS Laboratory, Thuwal 23955-6900, Saudi Arabia

ARTICLE INFO

Keywords:
A. Adhesive joints
B. Fracture toughness
C. Damage mechanics
D. Nondestructive testing
Bio-inspired adhesives

ABSTRACT

Herein, a novel adhesive joint that mimics the structure of the bondline of two biological systems that have excellent adhesion, *gecko* and *mytilus californianus*, was designed. Sacrificial cracks were embedded inside the adhesive layers to activate new dissipative mechanisms and thus increase the effective interlaminar fracture toughness. A finite element model (FEM) that considered the progressive damage in the adhesive layer and decohesion at both adhesive/adherend interfaces was used to understand the damage mechanisms of the bio-inspired adhesives. Contrary to classical joints that experience interfacial failure, wherein failure occurs at one of the substrate/adherend interfaces, our bio-inspired joints are characterized by crack bifurcation between both sides of the bondline. Thus the developed toughening ligaments cause the propagation of secondary and backward cracks at the lower and upper interfaces under and over the sacrificial cracks, respectively. Such crack branching and fragmentation together with the energy required to break these ligaments improve the effective toughness of the adhesive. Increasing the sacrificial crack width and gap between two successive cracks reduces the toughness through reduction in the allowed surface for secondary and backward crack propagation. The adhesive properties significantly affect this toughening effect that increases with adhesive strength and failure strain.

1. Introduction

Joining is a critical step in the fabrication of large structures. Ships and aircrafts are initially manufactured as small parts that are joined with each other to form the final complex structure, in which the joint is often the weakest part. Bolts and rivets are frequently used to join metals and composites [1]. The effectiveness of these mechanical systems is controversial in the case of composites because the holes drilled to fix bolts and rivets destroy the load-bearing fibers, produce large stress localization, and hence lower the resistance of the main structure. Full adhesive bonding can eliminate the use of mechanically interlocked systems (bolts or rivets would be avoided). However, adhesive joints generate brittle response, which causes safety and maintenance concerns. Moreover, the non destructive testing limitations for detecting adhesive flaws as kissing bonds remains a major issue that limits the use of an adhesive joint for structural applications [2,3]. Thus, better adhesive joints, with more progressive damage development, would be needed. Several techniques have been developed to improve the damage tolerance of composite joints, such as interleaving [4,5], stitching [6,7], z-pinning [8,9], adherend treatment [10–13], and thermoplastic and natural fiber inclusions [14–17]. However, these techniques require modifications in the composite structure, which might affect the in-plane strength of the composite [9].

Biomimetic engineering applies design principles found in nature to engineered materials and structures [18–20]. For example, researchers have mimicked the nanoscale design of seashell nacre for designing composite laminates with improved toughness [21–25]. Other designs of composite laminates are inspired by trees and their ability to distribute strains inside the cell walls of wood [26,27]. Researchers have been also inspired by bones and trees to improve the interfacial bonding of joints [28–30].

Gecko and *mytilus californianus* possess mechanisms through which they can considerably increase adhesion. For example, *geckos* exhibit extraordinary adhesion ability both on smooth and rough surfaces even when inclined [31]. The presence of concave nanospatula on the legs of the *gecko* allows the formation of cavities between the leg surface and the substrate (Fig. 1 (a)). These cavities result in high deformability with good bonding [32,33]. The bondline achieved in the *gecko* adhesion system is depicted in Fig. 1 (a). Another example of biological adhesion systems is found in *mytilus californianus* that exhibits excellent bonding with high adhesion strength in the deep water [34]. The adhesion system of *mytilus californianus* is based on the injection of proteins from the

* Corresponding author.
E-mail addresses: ahmed.abdelhady.1@kaust.edu.sa (A. Wagih), gilles.lubineau@kaust.edu.sa (G. Lubineau).

https://doi.org/10.1016/j.compositesa.2021.106530
Received 27 February 2021; Received in revised form 18 May 2021; Accepted 16 June 2021
Available online 29 June 2021
1359-835X/

plaque to bind the threads to the substrate. The adhesive protein layer features many porosities and voids, as shown in Fig. 1 (b). These voids toughen the bond because failure occurs through the breaking of the protein layer instead of the adhesive/substrate interface.

Inspired by these two biological adhesion systems, we present a novel bio-inspired structure of the bondline between materials that improves toughness. Our bio-inspired adhesive simulates the adhesion bondline of these systems, wherein tailored defects, i.e., sacrificial cracks, are generated in the bondline. We demonstrate the efficiency of this approach for composites used in critical applications that require excellent bonding properties.

To reveal the dissipation mechanisms generated in our bio-inspired adhesive, we utilized a finite element model (FEM) to simulate its response under double cantilever beam (DCB) tests and evaluated the resulting interlaminar fracture toughness. Unlike conventional models, in which a single layer of cohesive elements is applied to simulate the whole adhesive layer and all interfaces [35,36], we used multiscale numerical models to simulate the response of bio-inspired adhesives. Although the conventional strategy can efficiently simulate delamination inside composite laminates, wherein the adhesive thickness is zero and the delamination propagates through the mid-plane between two adjacent plies [37,38], it cannot accurately simulate thick adhesive layers, wherein energy dissipation occurs through plastic deformation of the adhesive layer. Moreover, the conventional strategy fails to consider complex dissipation mechanisms, such as bridging and adhesive failure. To overcome these limitations, researchers have developed multiscale numerical models that consider bridging [39,40] and adhesive layer thickness [41–43]. Here, we developed an FEM that defined the bondline as a bulk material with a progressive damage model. Moreover, we defined the interfaces with the adherends using two cohesive interfaces to allow crack propagation at interface in addition to the bifurcation between them. Then, parametric studies were performed to identify the most effective parameters influencing the toughness of the bio-inspired adhesive.

This article is organized as follows: Section 2, the bonding process of the developed bio-inspired adhesive, involving the generation of sacrificial cracks inside the adhesive, testing and implementation of the data reduction method that is explained. The FEM used to simulate the response of bio-inspired adhesives is also described. In Section 3, the numerical results are presented together with experimental validation obtained via testing. Finally, the toughening mechanisms in bio-inspired adhesives, the effect of crack topology, and adhesive properties are discussed, followed by conclusions being drawn in Section 4.

2. Methods

2.1. Manufacturing of bio-inspired adhesive joint

Unidirectional carbon/epoxy (T700/M21 Hexply, Hexcel) prepregs were used to manufacture adherends. The hand lay-up process was used to stack eight plies of 0.25 mm thickness each in a $[0°]_8$ stacking sequence resulting in a 2 mm adherend thickness. Compression molding was used to cure the manufactured plates (300 × 300 mm^2) under a pressure of 7 bar at 180 °C for 2 h using a hydraulic hot press. The heating and cooling rates were maintained constant at 3 °C/min.

After curing, the plates were cut into 250 × 110 mm^2 subplates using a water jet machine. Based on our previous work [44], we applied uniform laser treatment to the adherend surface using a pulsed CO_2 laser to improve adhesion between the adhesive and the adherend. For laser treatment a focal distance of 50 mm, spot diameter of 200 μm, speed of

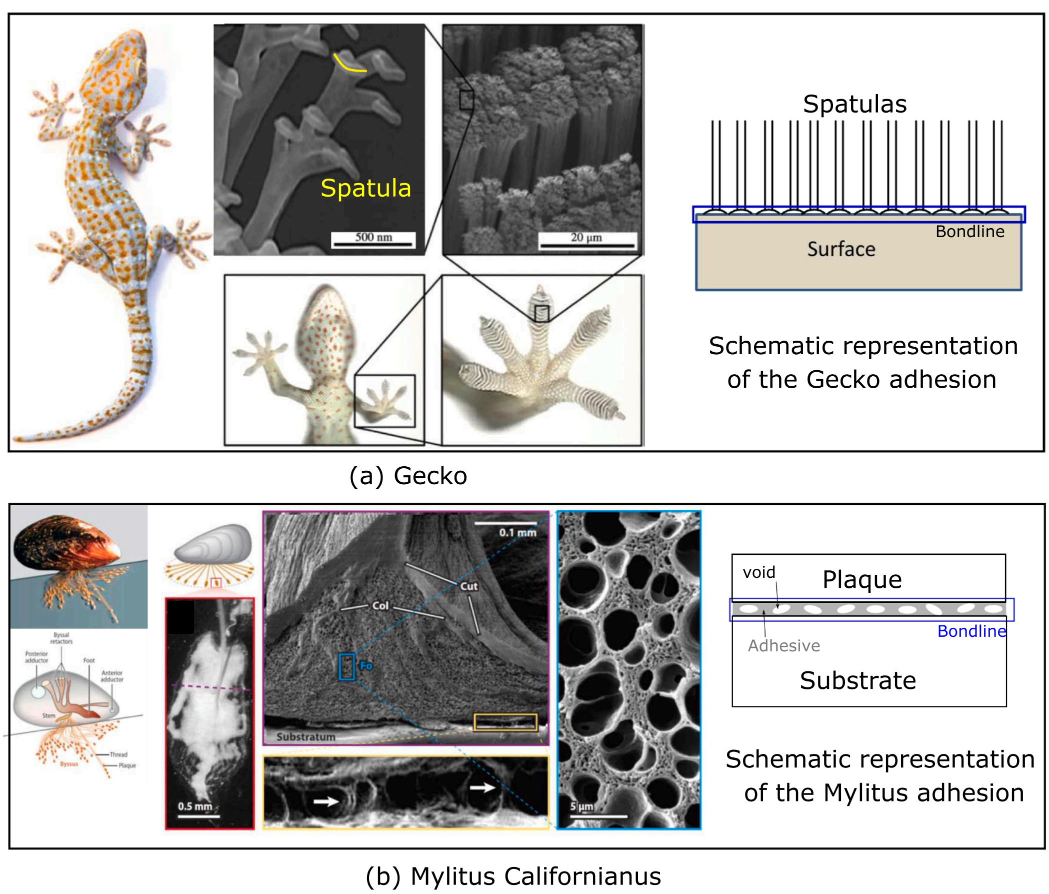

Fig. 1. Biological adhesion systems of (a) *gecko* [31] and (b) *mylitus californianus* [34]. Adapted from original references with modification and clarification with schematics [31,34]. (For interpretation of the references to color in this figure legend, the reader is referred to the web version of this article.)

1500 mm/s, pulse frequency of 60 kHz, and laser power of 22.5 W were used. Then, we submerged the subpanels for 10 min in acetone, dried them at 60 °C for 30 min, and air-cleaned them.

We used Araldite 420 A/B as the adhesive at a thickness of 0.4 mm to bond adherends. The manufacturing of our bio-inspired adhesive was done in four steps as illustrated in Fig. 2(a). The first step is the treatment of the adherends using laser as stated previously. The second step is the distribution of an equal amount of adhesive over each adherend reaching a thickness of 200 μm using a spatula leading approximately to an adhesive thickness of 400 μm. We also used copper wire of 400 μm diameter at the sub-plate edges to control the adhesive thickness. In the third step, we introduced a non-adhesive Polytetrafluoroethylene (PTFE) film of 18 μm thickness inside the adhesive bondline to create sacrificial cracks; we used a laser to cut the PTFE film into rectangular pieces of predefined width, c. Then, we placed the film with $c = 2$ mm and the gap between two successive films, g, on each adherend was 12 mm ($2g + c$), as shown in Fig. 2. A 60 mm long PTFE film was placed to generate the initial crack in the samples. In the fourth step, to generate offset form the mid-plane, h_c, of the sacrificial cracks with $h_c = 120$ μm, we placed copper wires (diameter; 120 μm) over one of the adherends at

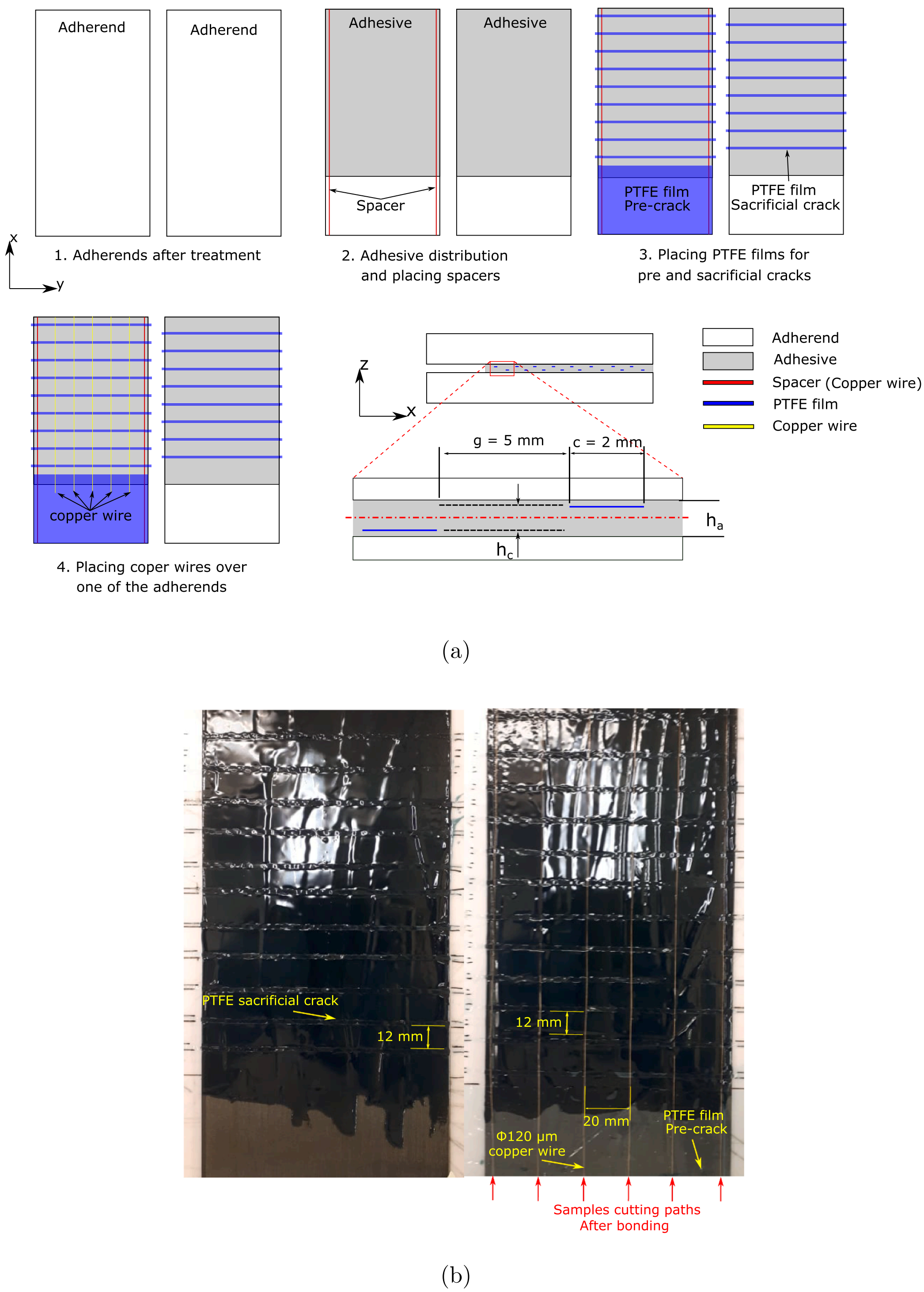

Fig. 2. Bonding process: (a) Schematic of the bio-inspired joint bonding steps and main geometrical parameters, (b) picture of the adherends during bonding. (For interpretation of the references to color in this figure legend, the reader is referred to the web version of this article.)

20 mm intervals across the plate width, as shown in Fig. 2. After bonding the two adherends, the PTFE film (with sacrificial cracks) was stretched from both sides. As the sample width was 20 mm, these copper wires were cut during sample cutting (marked with red arrows in Fig. 2(b)). After bonding, we placed the bonded sub-panels in furnace at 60°C for 30 min under vacuum and at the same temperature for 3 h without vacuum followed by holding at room temperature for 24 h.

2.2. Experimental tests

DCB tests were performed following the ASTM D5528-13 standard as shown in Fig. 3 to characterize the mode I interlaminar fracture toughness of our bio-inspired joint. The bonded sub-panels were cut into samples of 20 mm width and 150 mm length. Then, the samples were sprayed with white color to better visualize their damage mechanisms. Then, aluminum blocks were glued to the adherends using the same epoxy (Araldite 420) to enable load application (see Fig. 3). The tests were performed using a universal testing machine (Instron 2885) under displacement control at a loading rate of 1 mm/min. In-situ crack growth and damage mechanisms were monitored using a high-resolution camera (Canon EOS-1Ds). In total, three samples were tested for each configuration. The R-curve of the tested DCB specimen was obtained using Hashemi et al. [45] closed-form solution, wherein the beam compliance computed using the simple beam theory. The fracture toughness value, G_I, and the corresponding effective crack length, a_{eff}, were evaluated as:

$$G_I = \left[\frac{9}{4}\frac{P^4\cdot\delta^2}{B^3\cdot E_{xx}\cdot I}\right]^{\frac{1}{3}} \tag{1}$$

$$a_{eff} = \left[\frac{\delta\cdot B\cdot h^3\cdot E_{xx}}{8P}\right]^{\frac{1}{3}} - \zeta\cdot h \tag{2}$$

where P is the load, δ is the applied displacement at loading point, B is the sample width, E_{xx} is the in-plane modulus in the fiber direction, I is the second moment of area, h is the adherend thickness, and ζ is a correction factor that compensates for the assumption that the compliance at the crack root is zero; this differs from the real response in which some deflection and rotation occur at the crack tip [46,47]. ζ can be computed as:

$$\zeta = \left(\frac{E_{xx}}{11G_{xy}}\right)^{\frac{1}{2}}\left[3 - 2\left(\frac{\gamma}{1+\gamma}\right)^2\right]^{\frac{1}{2}} \tag{3}$$

where $\gamma = \frac{1.18}{G_{xy}}(E_{xx}\cdot E_{yy})^{\frac{1}{2}}$, E_{yy} is the in-plane modulus in the direction perpendicular to fiber direction and G_{xy} is the in-plane shear modulus.

2.3. Finite element modeling

We used a two-dimensional plane-strain (2D) FEM to predict load-displacement and R-curve responses of bonded joints loaded as DCB specimens. We modeled the real volume of the adhesive layer placed between two carbon fiber reinforced polymer (CFRP) adherends to enable the formation and propagation of damage mechanisms inside the adhesive and consider the existence of the adhesive thickness effect. The details of the model are specified in the following. The adherends, which are unidirectional T700/M21 CFRP laminates, were described using an orthotropic linear elastic model with E_{xx} = 125 GPa, E_{yy} = 7.8 GPa, G_{xy} = G_{xz} = 5.1 GPa, G_{yz} = 2.79, GPa, $\nu_{xy} = \nu_{xz} = 0.33$, and $\nu_{yz} = 0.4$ [40]. The adhesive's elastic response was described using isotropic linear elastic model. The elastic response continued until the yield strength, σ_y, was attained, following which isotropic hardening occurred until the ultimate strength, σ_u, was attained. Once the applied stress reached the adhesive strength, adhesive failure occurred following a slow linear softening until the damage variable equaled 0.15 in the ABAQUS built-in ductile damage evolution model; consequently, markedly faster softening occurred until the final failure, ϵ_f. The effects of critical strength and strain values were investigated and the chosen study values will be given later in this section. The stress-strain response of the adhesive is shown in Fig. 4. We utilized Q4 plane strain elements (CPE4R elements in the size of 0.1 mm) with reduced integration to mesh both the adherends and the adhesive.

We defined interfaces between the adherends and the adhesive by placing bilinear cohesive elements at the upper and lower interfaces. We used a maximum stress initiation criterion with the same critical stress σ_c

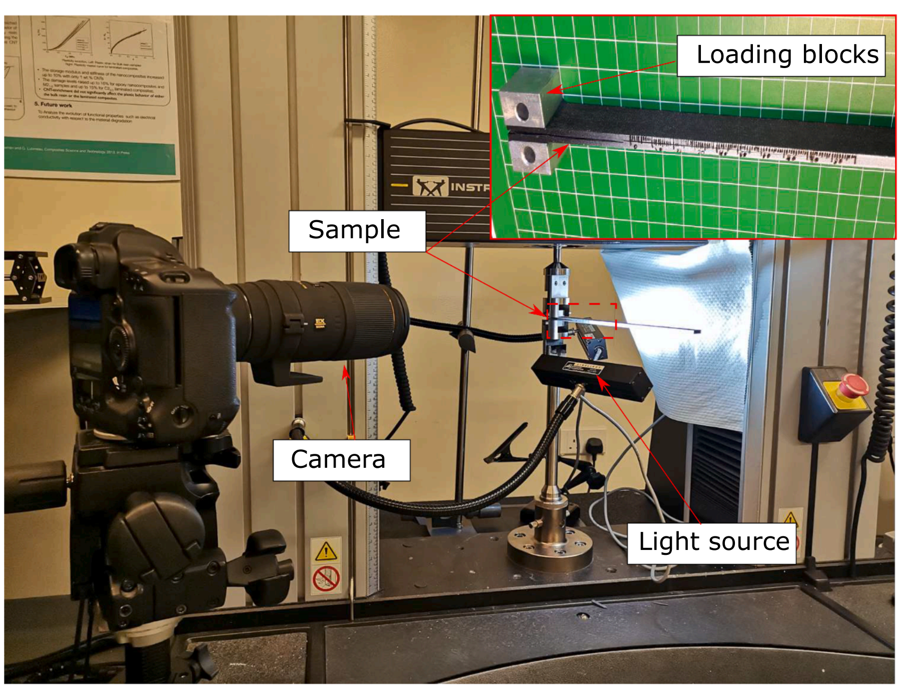

Fig. 3. Experimental DCB test set up. (For interpretation of the references to color in this figure legend, the reader is referred to the web version of this article.)

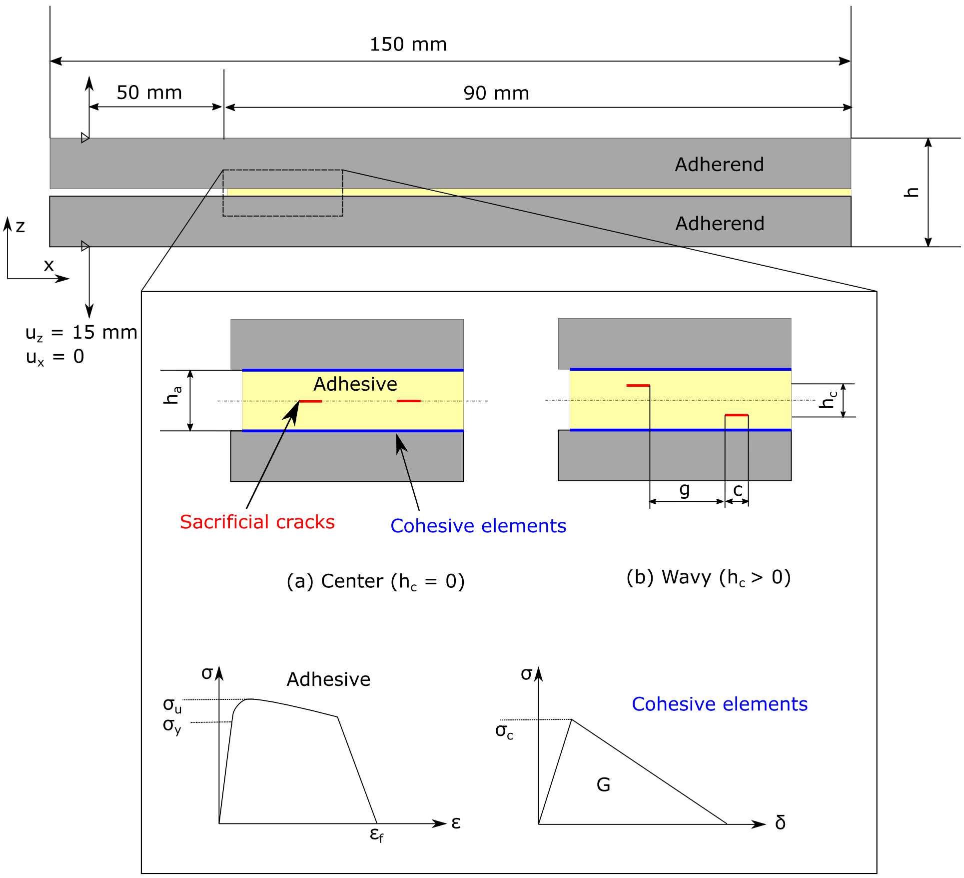

Fig. 4. Schematic of the 2D model with sacrificial cracks. The sacrificial cracks located at the center and that wave inside the adhesive layers are shown in the zoomed area together with the stress-strain response of the adhesive and traction separation law. (For interpretation of the references to color in this figure legend, the reader is referred to the web version of this article.)

in each mode. Therefore, once one of the stress components at both interfaces (normal or shear) reaches the critical stress, a crack initiates at that interface. Then, the crack propagation followed the mode independent criterion determined by the opening fracture energy G. The cohesive parameters, i.e., cohesive strength ($\sigma_c = 19$ MPa) and interface fracture energy ($G = 0.28$ N/mm), were characterized in an earlier study [48] via the three-point bending tests and DCB, respectively. The stiffness of the cohesive elements was obtained by dividing the adhesive stiffness by the cohesive element thickness, which gave the value of 1.5 $\times$ 10^7 Pa. Weak cohesive properties ($\sigma_c = 1$ MPa and $G = 0.01$ N/mm) were assigned to the first cohesive element at the lower interface (see Fig. 5(e)) to ensure crack initiation at this interface, which was guided by the precrack generated during experiments. Owing to the presence of sacrificial cracks, crack migration is expected between the upper and lower interfaces, thus generating adhesive ligaments.

The sacrificial crack seams inside the adhesive layer with length c were generated through the built-in ABAQUS model, leaving a gap (g) between two successive cracks. Herein, we considered that the sacrificial cracks had a vertical offset from the mid-plane, h_c. A special case was considered with centered cracks ($h_c = 0$), as shown in Fig. 4. The baseline model was built using the same modeling approach with cohesive elements defined at both interfaces. We verified the sensitivity of the model using coarse (16420 elements in the size of 0.2 mm), fine (39920 elements in the size of 0.1 mm), and very fine (77920 elements in the size of 0.05 mm) meshes.

The adherends, interfaces, and adhesive were divided as different features in a same ABAQUS part. Therefore, no interaction was specified between these structural components. Opening displacement (15 mm) was prescribed on the left ends of both upper and lower adherends and the right end was free of loadings, as shown in Fig. 4. The standard (static) implicit solver was used to solve the DCB problem considering the geometric nonlinearity.

Parametric studies were performed using the implemented model to study the effect of adhesive strength, failure strain, and adhesive layer topology (sacrificial crack width, the gap between two successive cracks, offset from the mid-plane, and adhesive thickness) on mode I fracture toughness. First, we studied the effect of the crack length, $c = 1$, 2, and 3 mm, and offset from the mid-plane, h_c = 0, 80, and 120 µm, for a constant gap of $g = 5$ mm.

Then, we studied the effect of different gap, $g = 5$, 10, and 15 mm, at a constant crack length ($c = 2$ mm). Then, the effect of varying adhesive thicknesses, h_a = 0.2 and 0.4 mm, was studied for samples with c = 2 mm and g = 5 mm. Finally, to study the effects of adhesive properties, the adhesive strength and strain were set as 0.5 and 2-fold those of Araldite 420 A/B (ultimate strength, $\sigma_u = 37$ MPa and failure strain, ϵ_f = 0.2), respectively. For the study of the adhesive strength, we kept the adhesive strain constant as 0.2. For the study of the adhesive failure strain, we kept the adhesive strength constant at 37 MPa. For the baseline joint, the elastic modulus and yield strength of the adhesive were constant (E = 1500 MPa, σ_y = 27 MPa and ν = 0.3) as extracted form the literature [40,49], except at σ_u = 18.5 MPa, where σ_y = 18 MPa.

The samples were identified based on their adhesive topology. For example, the sample with c = 2 mm, g = 5 mm and h_c= 120 µm was labeled "C2g5-hc120". The adhesive properties for all the simulations were defined as the properties of the real adhesive ($\sigma_u = 37$ MPa and ϵ_f = 0.2) unless stated otherwise. Additionally, the adhesive thickness was 0.4 mm for all configurations unless stated otherwise.

The R-curve of the simulated DCB specimen was obtained using the

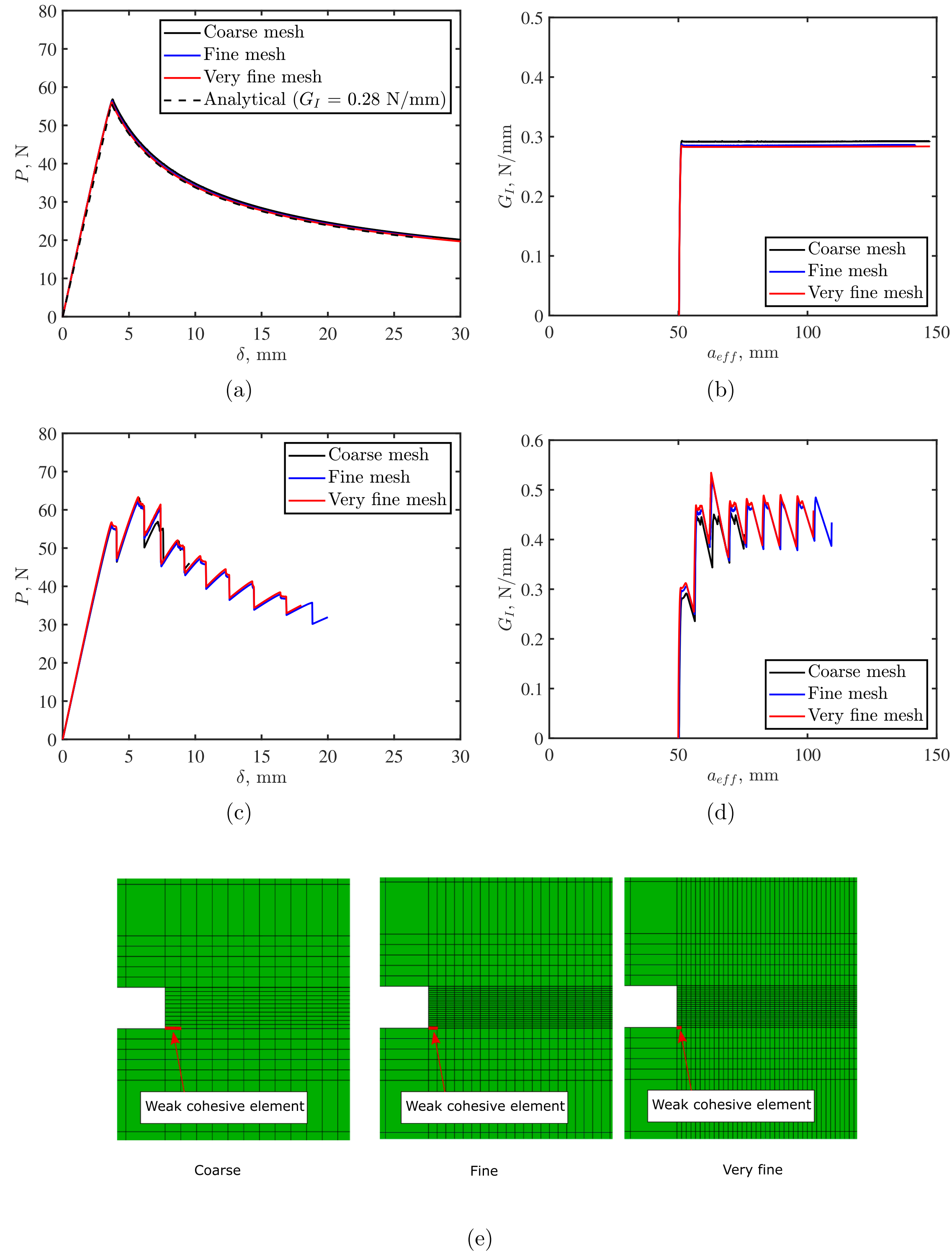

Fig. 5. Mesh sensitivity analysis: (a) and (b) load-displacement response and $G-a_{eff}$ curve of different meshes of baseline joint, (c) and (d) load-displacement response and $G-a_{eff}$ curve of different meshes of bio-inspired joint and (e) the different meshes considered. (For interpretation of the references to color in this figure legend, the reader is referred to the web version of this article.)

closed-form solution [45], which is explained in Section 2.2.

3. Results and discussion

3.1. Finite element model validation

Fig. 5 shows the load-displacement and R-curve for the DCB test simulation of the 0.4 mm-thick baseline adhesive joint (joint without sacrificial cracks) meshed using three different mesh sizes. The results were compared with the analytical solution presented in Eq. 1 for the crack propagation part of the curve, whereas the linear elastic part of the curve was compared with the linear elastic solution according to simple beam theory, $P = \frac{3E_{xx}I}{2(a_0+\zeta)^3}$ [47]. The figure shows that the response predicted using the coarse mesh deviates from the analytical solution;

however the response predicted using the fine and very fine meshes are identical (G_{Ic} = 0.2801 N/mm and 0.2804 N/mm for fine and very fine meshes) and fit well with the analytical solution. Moreover, the mesh sensitivity analysis for the bio-inspired joint shows that the fine and very fine mesh responses are identical. Therefore, we used the fine mesh for the whole simulations. It needs to be noted that interfacial cohesive elements exhibited higher normal stress compared to the shear stress (more than 30 times), indicating an opening dominant failure at interfaces.

Fig. 6 compares the FEM predictions and experimental load-displacement and R-curves for the baseline joint and bio-inspired joint with c = 2 mm, g = 5 mm, and h_c = 120 μm; an excellent correlation exists between predicted and experimental results for the baseline joint at the propagation stage because the interface toughness that was fed to the model was determined experimentally, and the average fracture toughness was 0.28 N/mm. However, at the initiation of the propagation, the simulation load and toughness were underestimated. This is due to the initiation of the crack at the adhesive layer mid-plane in the experiments, where the pre crack exists. Then, the crack propagates inside the adhesive layer until reaching the lower interface, which required more energy to propagate. However, in the simulation, we forced crack initiation at the lower interface. The model predicted the experimental load-displacement curve and R-curve of the bio-inspired joint well. The load-displacement curve and R-curve for the bio-inspired joint differed from those for the baseline joint, wherein the propagation load is relatively smooth for the baseline joint while it propagates in sawtooth shape for the bio-inspired joint. This difference between the global shape of the curves reflects the change in the crack propagation mechanisms.

3.2. Toughening mechanisms in the bio-inspired adhesive

Fig. 7 shows the load-displacement curve and R-curve of C2g5-hc120 together with the baseline joint with 0.4 mm adhesive thickness. The responses of both joints were identical in terms of elastic deformation and damage initiation up to “Point 1”. Following Point 1, the baseline joint exhibited smooth crack propagation at the lower interface resulting in a smooth R-curve. However, the bio-inspired joint exhibited load drops up to “Point 2” owing to the stiffness loss caused by the sacrificial crack. Between “Points 2 and 3”, crack propagation at the lower interface was inhibited, and the whole energy exerted was converted to elastic deformation of the adhesive layer which increase stress concentration at the upper interface. The stress concentration at that interface caused crack migration from the lower interface to the upper interface, forming two adhesive ligaments: one between the upper adherend and adhesive, and the other between the lower adherend and adhesive (Fig. 7(c)). These two ligaments increased the energy storage in the system through their elastic deformation. Additionally, two new dissipation mechanisms occurred owing to the adhesive’s plastic deformation. These mechanisms included crack propagation at the lower interface under the sacrificial crack, l_s, and the propagation of the backward crack at the upper interface over the sacrificial crack, l_b, as

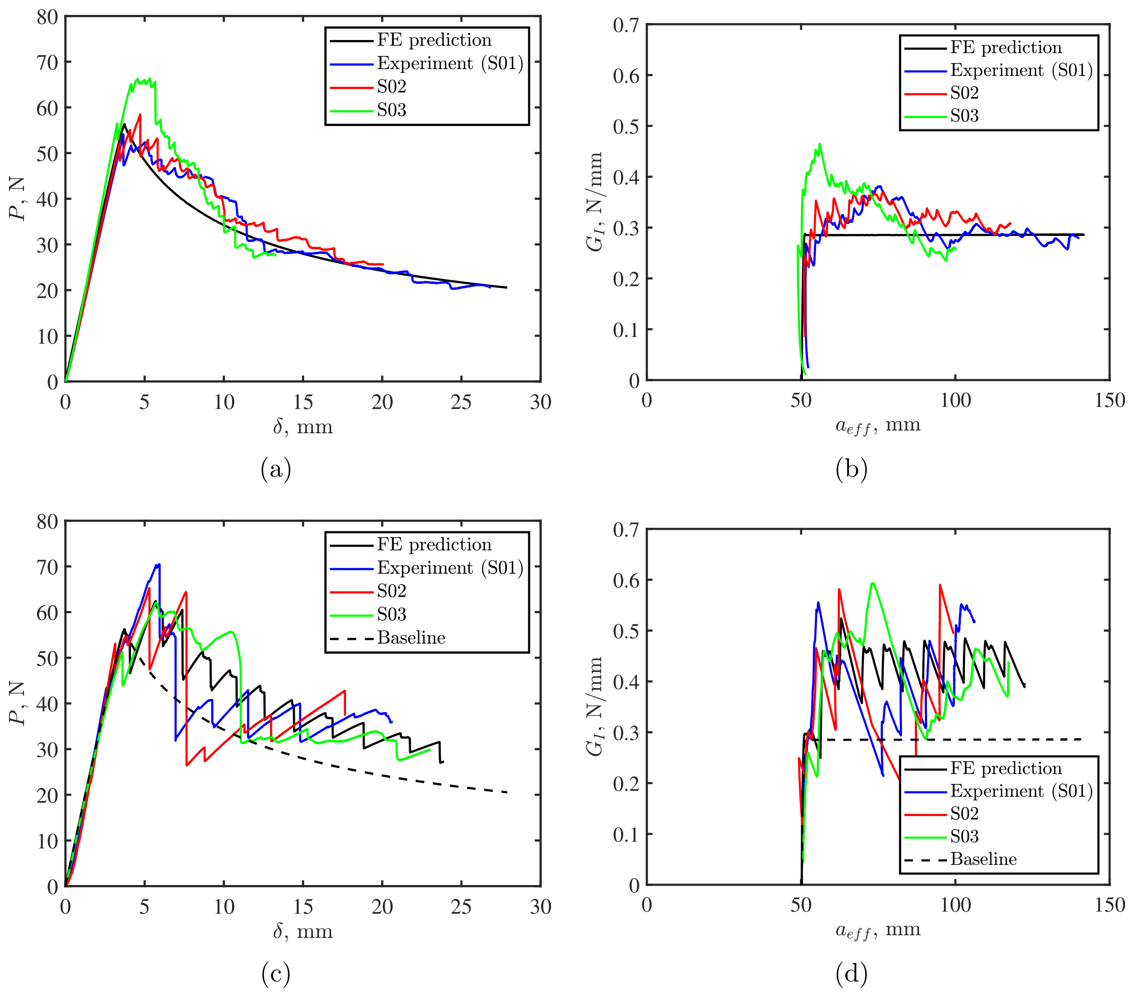

Fig. 6. Comparison between FEM and experimental results for the (a and b) baseline joint and (c and d) C2g5-hc120. S01, S02 and S03 refer to the three samples tested for each configuration. (For interpretation of the references to color in this figure legend, the reader is referred to the web version of this article.)

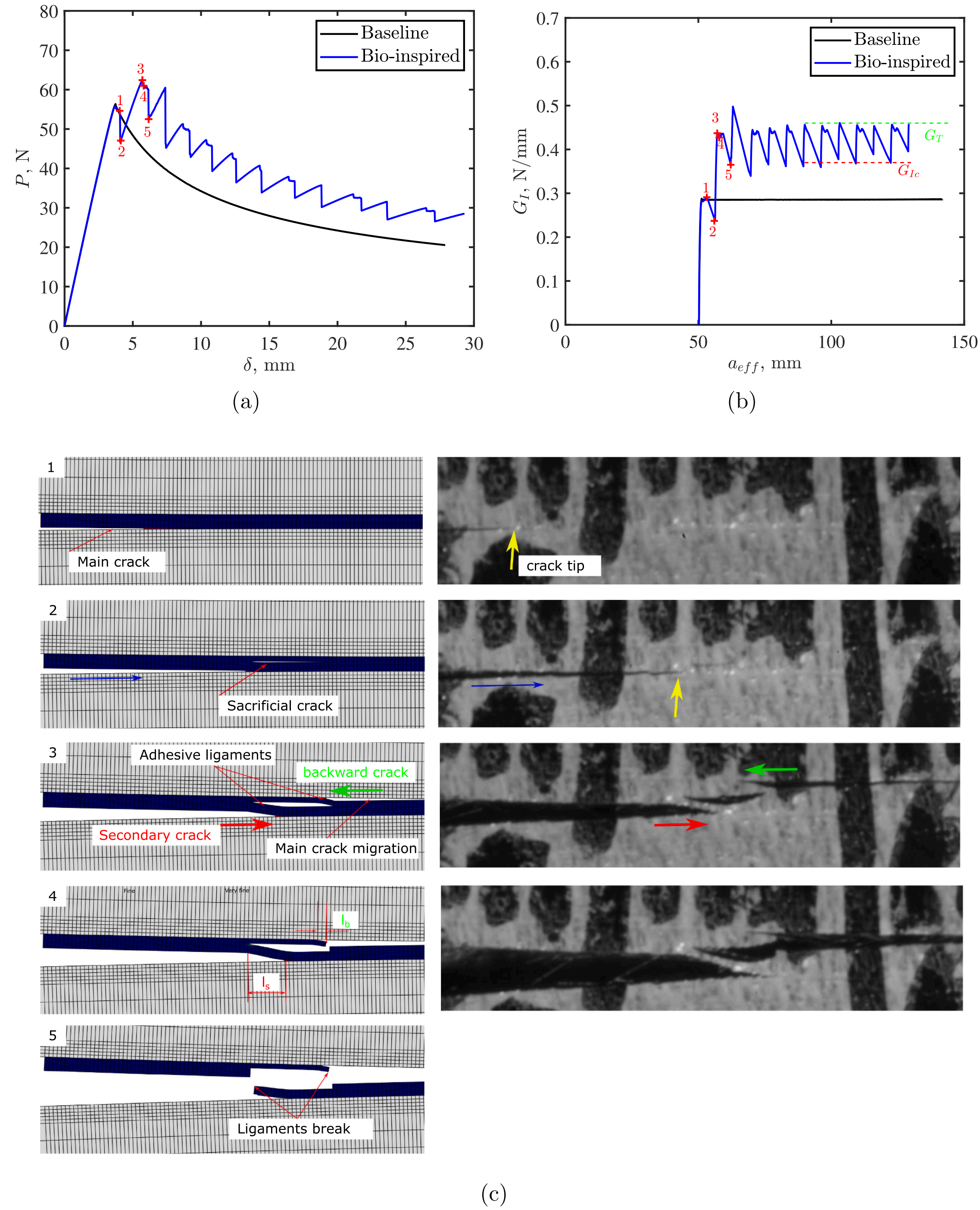

Fig. 7. Toughening mechanisms in bio-inspired adhesive joints (a) $P-\delta$ curve, (b) R-curve and (c) damage states corresponding to different points marked in a and b. The results correspond to the C2g5-hc120 joint with adhesive thickness of 0.4 mm. (For interpretation of the references to color in this figure legend, the reader is referred to the web version of this article.)

shown in Fig. 7(c). Altogether, crack migration, ligament deformation, secondary crack propagation, and backward crack propagation, increased the strain energy release rate from 0.23 N/mm at “Point 2” to 0.44 N/mm at “Point 3”, as shown in Fig. 7(b). The energy stored at “Point 3” includes the elastic energy of the ligament deformation that is recovered when the ligaments break. Notably, the damage mechanisms observed numerically at “Point 3” are identical to those observed experimentally as shown in Fig. 7(c).

After “Point 3”, the load decreased to “Point 4” owing to the breakage of the ligament between the upper interface and adhesive. Once this ligament was broken, the stored elastic energy was used to propagate the main and secondary cracks, thus compensating for the loss of the elastic energy; hence, slight load and energy reduction occurred. Additionally, part of the released energy is converted into kinetic energy that dissipates in the form of an elastic wave. After “Point 4” the system could dissipate energy in the secondary crack propagation until the lower ligament broke (Fig. 7(c)), resulting in a sudden load and energy drop, as shown in Figs. 7(a) and (b), respectively. Therefore, the energy at “Point 5” is the energy dissipated during the propagation of different damage mechanisms, including nonlocal mechanisms, the propagation of the secondary and backward cracks, kinetic energy dissipation in the form of elastic waves and ligament breakage. Although the ligament thickness was small, 0.4 mm, the energy required to break these ligaments was considerably higher than that required to propagate a crack at the interface; this is because the fracture energy of the adhesive was higher (3 N/mm [49]) that of the interface (0.28 N/mm). Thus, according to linear elastic fracture mechanics, the energy required to break a unit of the adhesive ligament was 10.7-fold larger than that required to propagate a crack at the interface.

Noteworthy, the proposed bio-inspired adhesive joint generated a safe response after the ligament broke. For example, after "Point 5", the energy for crack propagation increased from 0.37 to 0.5 N/mm, indicating an improvement compared to the baseline joint that generates an unstable response as shown in Fig. 7(a).

In the R-curve, for these bio-inspired adhesive joints, two toughness values are shown using green and red dashed lines in Fig. 7(b). The green line, G_T, represents the total energy in the system without ligament breakage. This value includes the elastic energy that is temporarily stored in the ligaments and does not fairly represent the dissipation in the joint. The red dashed line, G_{Ic}, represents the fracture energy dissipated via different damage mechanisms and gives the critical fracture energy of the system. Thus, the fracture toughness value is assigned based on a conservative value at the red line. This fracture toughness represent the energy dissipated at the minimum load after the load-drop in the load-displacement curve. However, the real toughness might be slightly larger if we consider the energy dissipated between the maximum and the minimum load after ligament break as discussed in previous works [50–52].

3.3. Influence of the bio-inspired adhesive's topology

Fig. 8 shows the effect of offset from the mid-plane, h_c, on the load-displacement curve, R-curve, and damage mechanisms in bio-inspired joints with 0.2 mm adhesive thicknesses. In addition, a baseline test for the same adhesive thickness was performed for comparison. For sacrificial cracks located at the center of the bondline, $h_c = 0$, cracks always propagated at the lower interface, inhibiting the formation of ligaments and hence the dissipation in the secondary and backward cracks. This case, $h_c = 0$, proves that ligaments formation generates high energy dissipation because if the energy dissipated via ligament plastic deformation and breakage is identical to crack propagation, then the load-displacement response and fracture energy should be lower than those of the baseline joint. The energy dissipated after 66 mm of crack propagation reached the same energy level as that of the baseline. However, in this case, 10 sacrificial cracks existed, indicating that the propagated crack path was reduced by 20 mm. Hence, the energy lost because of sacrificial cracks was compensated by the energy dissipated in the adhesive break. The summation of the adhesive breakage at 10 sacrificial cracks was 2 mm. Therefore, 2 mm propagation in the adhesive was equivalent to 20 mm propagation at the interface, highlighting the role of the adhesive break as an important source of energy dissipation in our bio-inspired joints.

For $h_c > 0$, the response was almost the same for $h_c = 80$ and 120 μm. This indicates that if the offset from the mid-plane is introduced to break the symmetry, crack migration occurs and adhesive ligaments are formed, resulting in secondary and backward crack propagation, which improves the system fracture energy, and the exact value of h_c is not significant. The total energy stored in the system before ligament break, G_T, was 0.37 N/mm, and the fracture energy, G_{Ic}, was 0.32 N/mm; this energy was 0.28 N/mm for the baseline joint. Notably, the energy exhibits progressive increase with increasing the effective crack length due to the accumulation of energy dissipated in adhesive ligament breakage.

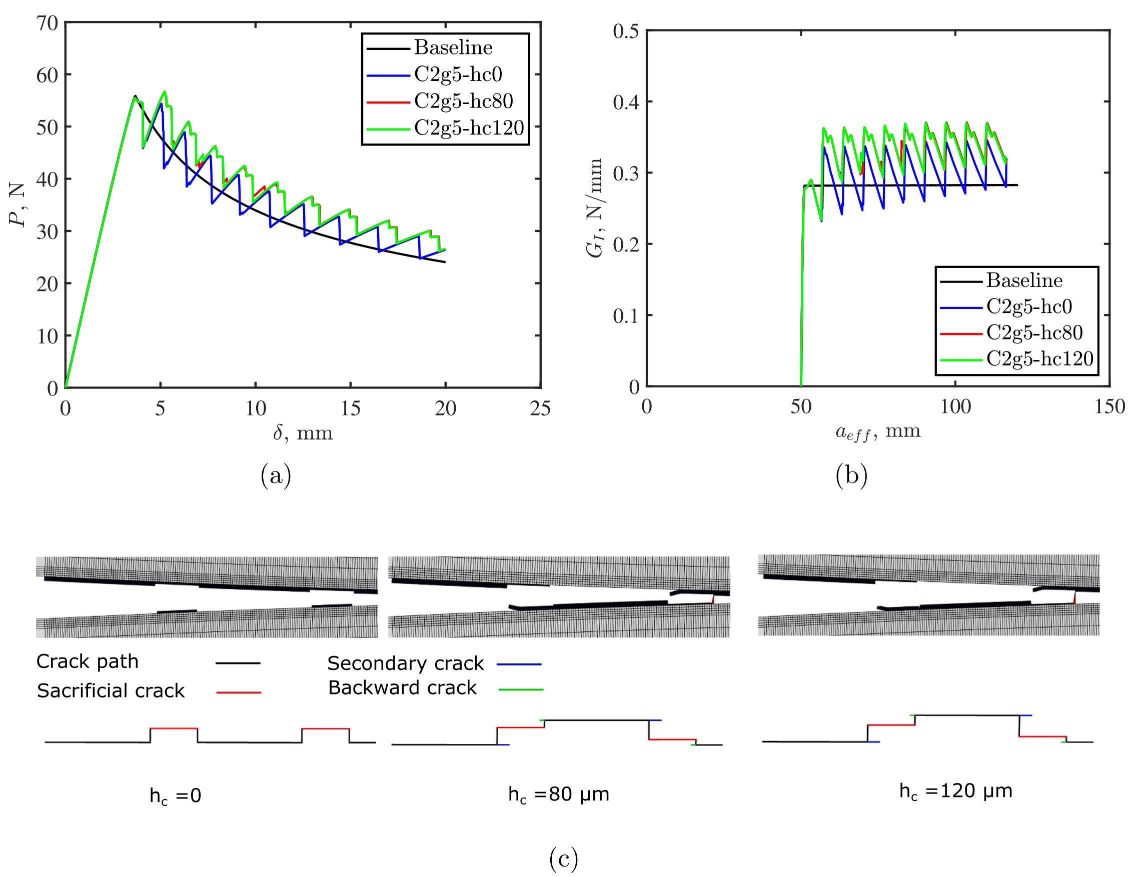

Fig. 8. Effect of sacrificial crack offset from the mid-plane, h_c, on the response of bio-inspired adhesive joints (a) $P-\delta$ curve, (b) R-curve, and (c) the state of damage corresponding to different h_c and a schematic representation of the crack path. The results correspond to a joint with adhesive thickness of 0.2 mm. (For interpretation of the references to color in this figure legend, the reader is referred to the web version of this article.)

Comparing the total and fracture energy of C2g5-hc120 obtained at adhesive thicknesses of 0.2 and 0.4 mm, respectively, revealed higher total and fracture energies for the latter thickness (Fig. 7(b) and 8(b)). This is because of the larger volume of adhesive breaking when the adhesive is thicker, which dissipates more energy. Moreover, thick ligaments formed in the thick adhesives break at a higher load, enabling further propagation of the secondary and backward cracks, $l_s = 0.9$ and 0.4 mm and $l_b = 0.2$ and 0.1 mm for thick and thin adhesives, respectively.

The effect of the sacrificial crack length, c, on the $P-\delta$ and R-curve of the bio-inspired composite with an offset from the mid-plane of $h_c = 120$ μm and adhesive thickness of 0.4 mm is shown in Figs. 9(a) and (b). Increasing c reduces the maximum load and mode I toughness of the joint through the reduction of the energy dissipated in nonlocal damage mechanisms, crack migration, secondary and backward cracks, and ligament break. The increased c reduces the number of ligaments formed as well as secondary and backward cracks, which reduces the global energy dissipated by the system. Moreover, for small c, the allowed area for crack propagation increases, thereby increasing the fracture toughness. Therefore, the activation of the nonlocal damage mechanisms is associated with the presence of cracks rather than the crack length. After a sacrificial crack is generated, even at a length of 1 mm, the nonlocal damage mechanisms are activated and higher energy dissipation occurs, improving the fracture toughness. Notably, the total energy, G_T, is reduced with increasing c owing to the reduction in the number of broken ligaments that store the elastic energy.

The effect of the gap between two successive sacrificial cracks, g, on the DCB response of the bio-inspired joint is shown in Figs. 9(c) and (d). As expected, increasing g reduces the interlaminar fracture toughness due to the reduction in the number of ligaments formed. This improvement in fracture toughness is proportional to the number of broken ligaments, the length of secondary and backward cracks, and the total length allowed for crack propagation. Increasing g increases the allowed length for crack propagation, which improves fracture toughness. However, it reduces the generation of nonlocal damage mechanisms expressed by the number of crack migrations and ligaments, which prevents fracture toughness improvement. The negative effect of increasing g (the reduction in the number of ligaments) is larger than the positive effect (increasing allowed crack propagation area) in which the fracture toughness globally decreases. Therefore, for the current analysis, a joint with small c and small g, C1g5, exhibits the best G_{Ic} improvement (67%) over that of the baseline, achieving $G_{Ic} = 0.47$ N/mm against ($G_{Ic} = 0.28$ N/mm).

3.4. The effect of adhesive properties on a bio-inspired joint

The adhesive's mechanical properties can be easily tailored in bonded joints owing to the availability of commercial adhesives with distinct properties and the ability to tailor certain properties, such as strength or failure strain, using different materials: e.g., ceramics [53,54], metals [55], and thermoplastics inclusions [56–58]. The effect of adhesive strength, σ_u, and failure strain, ϵ_f, on the DCB response of

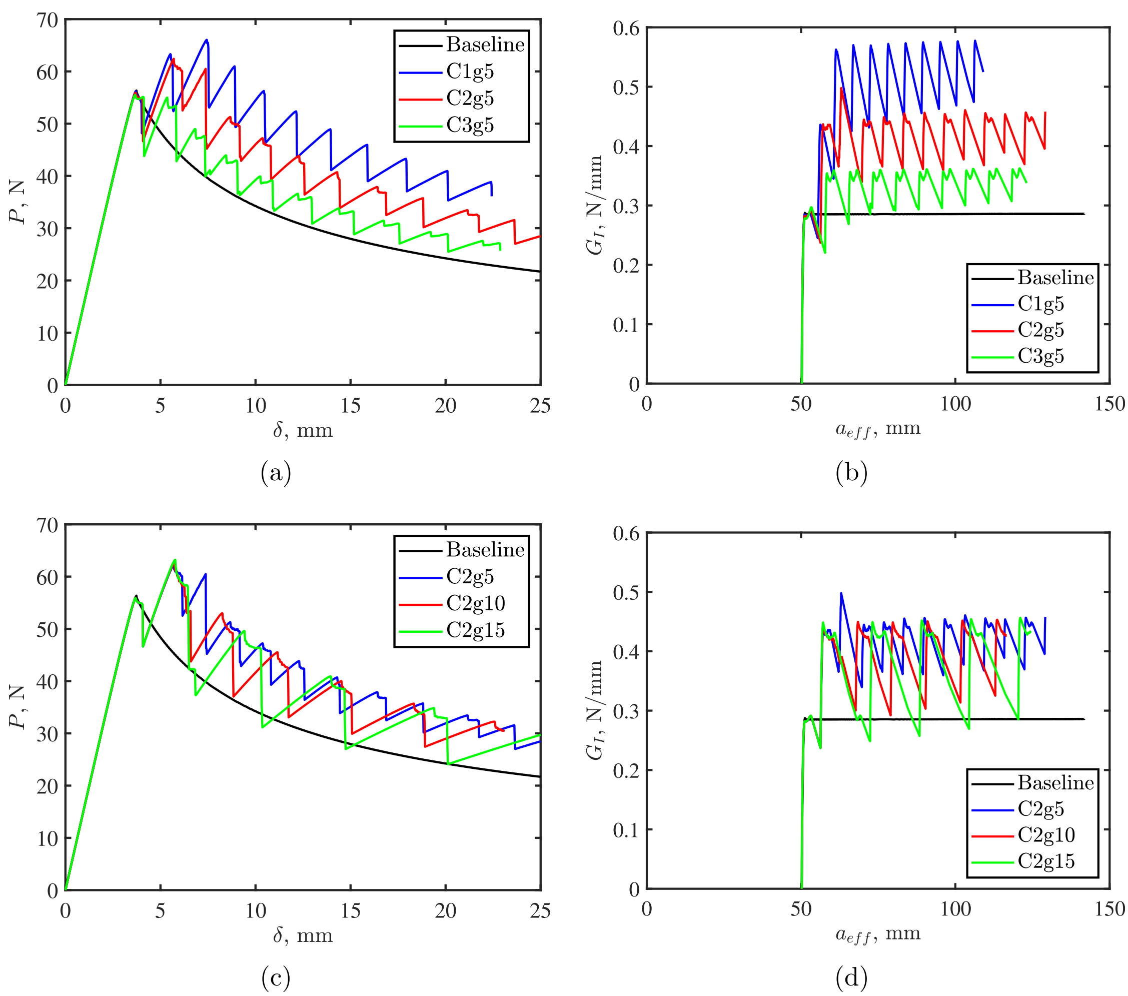

Fig. 9. Effect of the sacrificial crack width, c, and the gap between two sacrificial cracks, g, on the response of bio-inspired adhesive joints with $h_c = 120$ μm and $h = 0.4$ mm (a and b) effect of c and g on $P-\delta$ and R-curve (c and d). (For interpretation of the references to color in this figure legend, the reader is referred to the web version of this article.)

C2g5-hc120 is shown in Figs. 10 and 11, respectively. These figures show the significant effect of both properties on the $P-\delta$ and R-curve responses. The joint maximum load and fracture toughness are proportional to the adhesive strength. Doubling the adhesive strength from 37 MPa (Araldite adhesive strength) to 74 MPa improves the fracture toughness from 0.36 to 0.74 N/mm. In the current bio-inspired joint, the nonlocal damage mechanisms result from crack migration to the other interface (Section 3.2) and create an adhesive ligament that prominently participates in the dissipation. Doubling the adhesive strength inhibits ligament break and allows larger propagation of secondary and backward cracks, as shown in Fig. 10(c). For the largest adhesive strength, $\sigma_u = 74$ MPa, the secondary and backward cracks equal $l_s = 7$ mm and $l_b = 1.0$ mm, compared to $l_s = 0.9$ mm and $l_b = 0.2$ mm for the adhesive with a strength of 37 MPa. Reducing the adhesive strength to half, 18.5 MPa, makes it lower than the strength of the baseline joint, causing earlier breakage of the ligament before the propagation of the secondary and backward cracks. Therefore, despite the crack migrating to the other interface, the secondary and backward cracks do not propagate, and the only extra dissipation mechanism is ligament breakage as shown in Fig. 10(c). In this case, owing to the adhesive's lower strength, the energy required to break these ligaments is relatively small; thus, the global fracture energy is slightly smaller than that of the baseline joint.

The effect of adhesive failure strain on the $P-\delta$ and R-curve responses of the bio-inspired joint is shown in Fig. 11. Increasing the failure strain improves the $P-\delta$ and R-curve responses. Increasing the failure strain to 0.4 increases the joint maximum load to 81.4 N compared to 62.1 N and 55.6 N for the bio-inspired joint with a failure strain of 0.2 and the baseline joint, respectively. Moreover, G_{Ic} increased to 1.04 N/mm compared to 0.36 and 0.28 N/mm for the bio-inspired joint with a failure strain of 0.2 and the baseline joint, respectively. This improvement is attributed to the higher failure strain of the ligaments, which allows larger ligament deformation. Therefore, larger propagation of the secondary and backward cracks occurs, $l_s = 7$ mm and $l_b = 1.6$ mm, dissipating more energy and thus improving the fracture toughness. Decreasing the failure strain to 0.1 reduces the deformability of the adhesive ligaments, causing earlier ligament breakage. Therefore, the secondary crack propagation is very small, $l_s = 0.1$ mm, whereas the backward crack propagation is inhibited, causing lower energy dissipation and hence lower fracture toughness, $G_{Ic} = 0.28$ N/mm; this fracture toughness is lower than that of the bio-inspired joint with a failure strain of 0.2 and equal to that of the baseline joint.

Our results showed that the fracture toughness of the bio-inspired joint can be tailored by changing either the adhesive strength or failure strain. These two properties can be easily tailored using thermoplastics, metals, and ceramics and enable the designing of bonded joints with different toughness values using the same adhesive. The fracture toughness of the same adhesive can be increased by 264 % by strengthening the proposed bio-inspired adhesive with factor of 2. Moreover, the toughness can be increased by 371 % by increasing the failure strain by a factor of 2. Additionally, the toughness can be adjusted for specific applications at a certain level by controlling both parameters. It is valuable noting that for adhesives with very high failure strain or strength, where long bridging occurs as shown in Fig. 10(c), the failure process zone is very large reaching the material characteristic

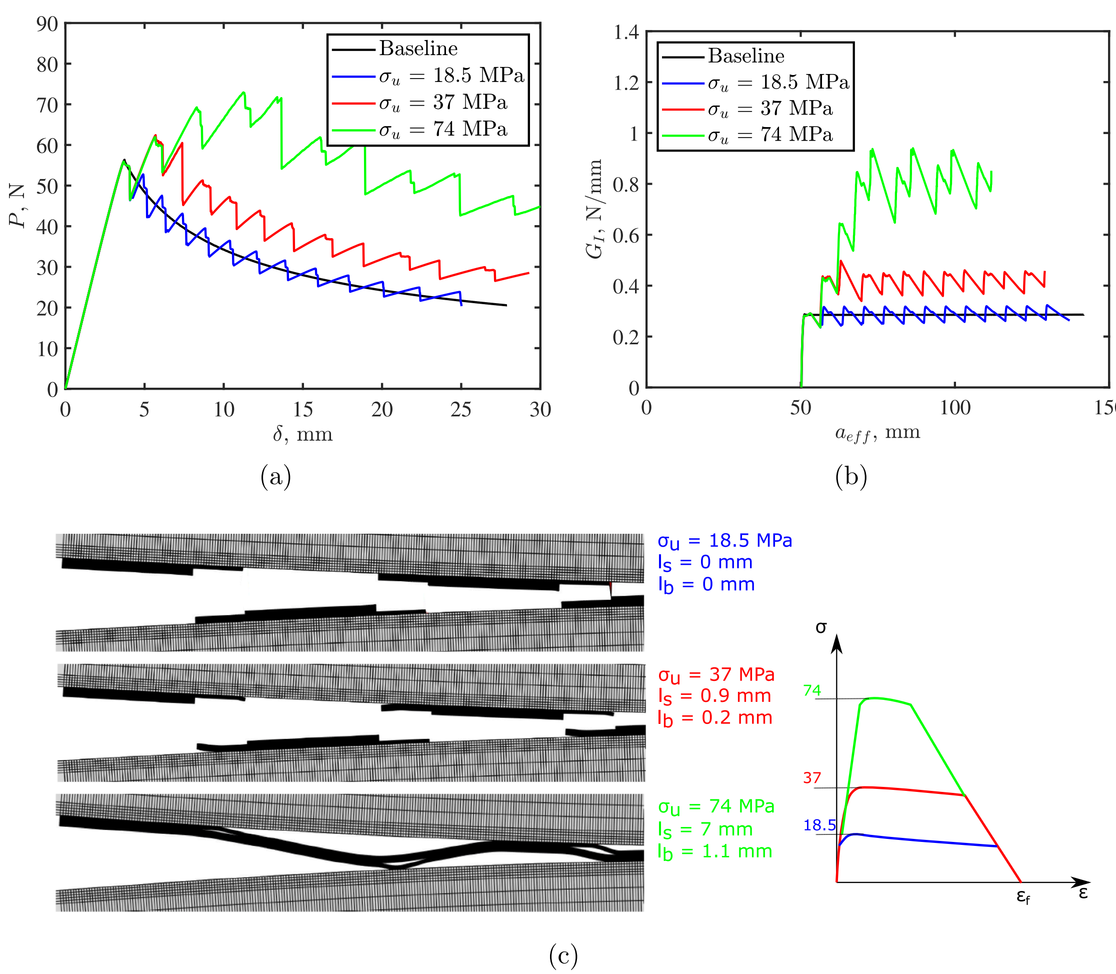

Fig. 10. Effect of adhesive strength on the response of C2g5-hc120 with 0.4 mm thickness (a) $P-\delta$ curve, (b) R-curve, and (c) damage evolution maps for different strengths. (For interpretation of the references to color in this figure legend, the reader is referred to the web version of this article.)

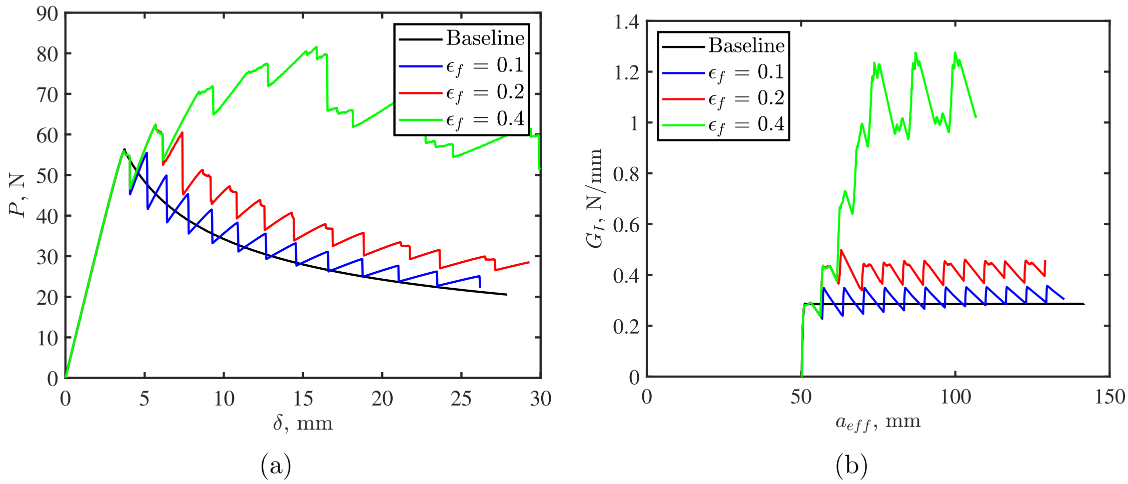

Fig. 11. Effect of adhesive failure strain on the response of C2g5-hc120 with a thickness of 0.4 mm (a) $P-\delta$ curve and (b) R-curve. (For interpretation of the references to color in this figure legend, the reader is referred to the web version of this article.)

length. In this case, the linear elastic fracture mechanics laws became inapplicable anymore and nonlinear mechanics laws such as J-integral and cohesive models should be applied to characterize the interface properties [59]. Thus, the crack propagation response become a function of the geometry of the joint and hence caution should be considered for fracture toughness characterization of the joint and application of different toughness tests such as DCB and climbing drum peel tests should be performed [51].

4. Conclusions

Herein, we developed a novel bio-inspired adhesive joint with improved interlaminar fracture toughness by generating sacrificial cracks inside the adhesive layer with specific topology that activates nonlocal dissipation damage mechanisms through the development of bridging ligaments. We simulated the DCB test of our bio-inspired adhesive joint using a 2D FEM, that considers the simulation of the adhesive layer as a bulk material with linear elastic response followed by the application of the softening law until complete failure. The model also considers debonding at both adhesive/adherend interfaces according to bilinear cohesive law. The presented model was validated with the experimental results for conventional and bio-inspired joint of CFRP plates developed in the study.

The results show that the damage mechanisms in our proposed bio-inspired adhesive differ from those of baseline adhesive joints. Unlike conventional adhesive joints, wherein the crack propagates at the lower adhesive/adherend interface, the crack migrates to the upper interface at the sacrificial crack position in the bio-inspired adhesive. This crack migration allows the formation of the adhesive ligament between the upper and lower adherends and the adhesive, leading to the propagation of a secondary crack at the lower interface under the sacrificial crack together with the propagation of a backward crack at the upper interface over the sacrificial crack. The simultaneous propagation of these two cracks, dissipates more energy during fracture. Moreover, when the ligament deformation reaches its maximum deformability, it breaks, dissipating more energy. Therefore, in our bio-inspired adhesive, we activate three dissipation mechanisms, secondary and backward crack propagation and ligament breakage, which increase the energy dissipation and improve fracture toughness. Decreasing the sacrificial crack width and gap between two successive cracks improves the toughness due to the increase in the allowable surface for secondary and backward crack propagations. The adhesive properties significantly affect the toughness of the bio-inspired adhesives, wherein toughness increases with increasing adhesive strength and failure strain.

The proposed bio-inspired adhesive demonstrated herein can improve the interlaminar fracture toughness of bonded joints and provide progressive damage manner of the joint, thus improving safety and toughness in structural composite applications. However, from applicability point of view for real-life structure bonding, more research has to be done to simplify the manufacturing process. Moreover, the possibility of using random cracks inside the adhesive because the major requirement of the technique is to break the symmetry of the sacrificial cracks (by introducing the crack offset, h_c), which might simplify the manufacture process needs to be investigated.

CRediT authorship contribution statement

A. Wagih: Conceptualization, Methodology, Supervision, Investigation, Data curation, Writing – original draft, Writing – review & editing. **R. Tao:** Investigation, Data curation, Writing – original draft, Writing – review & editing. **G. Lubineau:** Conceptualization, Methodology, Supervision, Writing – original draft, Writing – review & editing.

Declaration of Competing Interest

The authors declare that they have no known competing financial interests or personal relationships that could have appeared to influence the work reported in this paper.

Acknowledgment

This research was funded by King Abdullah University of Science and Technology (KAUST) Office of Sponsored Research (OSR) under award number OSR-2017-CRG6-3388.01.

References

[1] Ageorges C, Ye L, Hou M. Advances in fusion bonding techniques for joining thermoplastic matrix composites: a review. Compos Part A: Appl Sci Manuf 2001;32(6):839–57.
[2] Jeenjitkaew C, Guild F. The analysis of kissing bonds in adhesive joints. Int J Adhes Adhes 2017;75:101–7.
[3] Michaloudaki M, Lehmann E, Kosteas D. Neutron imaging as a tool for the non-destructive evaluation of adhesive joints in aluminium. Int J Adhes Adhes 2005;25(3):257–67.
[4] Beckermann GW, Pickering KL. Mode I and mode II interlaminar fracture toughness of composite laminates interleaved with electrospun nanofibre veils. Compos Part A: Appl Sci Manuf 2015;72:11–21.
[5] Narducci F, Lee K-Y, Pinho S. Interface micro-texturing for interlaminar toughness tailoring: a film-casting technique. Compos Sci Technol 2018;156:203–14.
[6] Jain LK, Dransfield KA, Mai Y-W. On the effects of stitching in CFRPs-II. Mode II delamination toughness. Compos Sci Technol 1998;58(6):829–37.
[7] Mouritz AP, Cox B. A mechanistic approach to the properties of stitched laminates. Compos Part A: Appl Sci Manuf 2000;31(1):1–27.

[8] Chang P, Mouritz A, Cox B. Properties and failure mechanisms of pinned composite lap joints in monotonic and cyclic tension. Compos Sci Technol 2006;66(13):2163–76.

[9] Mouritz AP. Review of z-pinned composite laminates. Compos Part A: Appl Sci Manuf 2007;38(12):2383–97.

[10] Fischer F, Kreling S, Jäschke P, Frauenhofer M, Kracht D, Dilger K. Laser surface pre-treatment of CFRP for adhesive bonding in consideration of the absorption behaviour. J Adhes 2012;88(4–6):350–63.

[11] Tao R, Alfano M, Lubineau G. In situ analysis of interfacial damage in adhesively bonded composite joints subjected to various surface pretreatments. Compos Part A: Appl Sci Manuf 2019;116:216–23.

[12] Tao R, Alfano M, Lubineau G. Laser-based surface patterning of composite plates for improved secondary adhesive bonding. Compos Part A: Appl Sci Manuf 2018;109:84–94.

[13] Ramaswamy K, O'Higgins RM, Kadiyala AK, McCarthy MA, McCarthy CT. Evaluation of grit-blasting as a pre-treatment for carbon-fibre thermoplastic composite to aluminium bonded joints tested at static and dynamic loading rates. Compos Part B: Eng 2020;185:107765.

[14] Löbel T, Holzhüter D, Sinapius M, Hühne C. A hybrid bondline concept for bonded composite joints. Int J Adhes Adhes 2016;68:229–38.

[15] Heide-Jørgensen S, de Freitas ST, Budzik MK. On the fracture behaviour of CFRP bonded joints under mode I loading: Effect of supporting carrier and interface contamination. Compos Sci Technol 2018;160:97–110.

[16] Delzendehrooy F, Ayatollahi M, Akhavan-Safar A, da Silva L. Strength improvement of adhesively bonded single lap joints with date palm fibers: Effect of type, size, treatment method and density of fibers. Compos Part B: Eng 2020;188:107874.

[17] Saraç İ, Adin H, Temiz Ş. Investigation of the effect of use of Nano-Al_2O_3, Nano-TiO_2 and Nano-SiO_2 powders on strength of single lap joints bonded with epoxy adhesive. Compos Part B: Eng 2019;166:472–82.

[18] Chen P-Y, Lin A, Lin Y-S, Seki Y, Stokes A, Peyras J, et al. Structure and mechanical properties of selected biological materials. J Mech Behav Biomed Mater 2008;1(3):208–26.

[19] McKittrick J, Chen P-Y, Tombolato L, Novitskaya E, Trim M, Hirata G, et al. Energy absorbent natural materials and bioinspired design strategies: a review. Mater Sci Eng C 2010;30(3):331–42.

[20] Meyers MA, Chen P-Y, Lin AY-M, Seki Y. Biological materials: structure and mechanical properties. Prog Mater Sci 2008;53(1):1–206.

[21] Dutta A, Tekalur SA. Synthetic staggered architecture composites. Mater Des 2013;46:802–8.

[22] Tang Z, Kotov NA, Magonov S, Ozturk B. Nanostructured artificial nacre. Nat Mater 2003;2(6):413–8.

[23] Munch E, Launey ME, Alsem DH, Saiz E, Tomsia AP, Ritchie RO. Tough, bio-inspired hybrid materials. Science 2008;322(5907):1516–20.

[24] Bonderer LJ, Studart AR, Gauckler LJ. Bioinspired design and assembly of platelet reinforced polymer films. Science 2008;319(5866):1069–73.

[25] Melaibari A, Wagih A, Basha M, Kabeel A, Lubineau G, Eltaher M. Bio-inspired composite laminate design with improved out-of-plane strength and ductility. Compos Part A: Appl Sci Manuf 2021;144:106362.

[26] Greenhalgh E, Lewis A, Bowen R, Grassi M. Evaluation of toughening concepts at structural features in CFRP-Part I: stiffener pull-off. Compos Part A: Appl Sci Manuf 2006;37(10):1521–35.

[27] Mattheck CM, Mattheck C. Design in nature: Learning from trees. Springer Science & Business Media; 1998.

[28] Munzinger M, Kraft O, Mattheck C. Computer aided adhesive and assembly optimization method: Biomimetic optimization of adhesive joints. J Mater Res 2006;21(8):2011–7.

[29] Burns L, Mouritz AP, Pook D, Feih S. Bio-inspired hierarchical design of composite T-joints with improved structural properties. Compos Part B: Eng 2015;69:222–31.

[30] Akrami R, Fotouhi S, Fotouhi M, Bodaghi M, Clamp J, Bolouri A. High-performance bio-inspired composite T-joints. Compos Sci Technol 2019;184:107840–51.

[31] Izadi H, Zandieh A, Penlidis A. Bio-inspired dry adhesives: Contact electrification and electrostatic interactions. Kirk-Othmer Encycl Chem Technol 2000:1–35.

[32] Jeong J, Kim J, Song K, Autumn K, Lee J. Geckoprinting: Assembly of microelectronic devices on unconventional surfaces by transfer printing with isolated gecko setal arrays. J Roy Soc Interface 2014;11(99):20140627.

[33] Tao D, Wan J, Pesika NS, Zeng H, Liu Z, Zhang X, et al. Adhesion and friction of an isolated gecko setal array: The effects of substrates and relative humidity. Biosurface Biotribol 2015;1(1):42–9.

[34] Lee BP, Messersmith PB, Israelachvili JN, Waite JH. Mussel-inspired adhesives and coatings. Annu Rev Mater Res 2011;41:99–132.

[35] Malkin R, Trask RS, Bond IP. Control of unstable crack propagation through bio-inspired interface modification. Compos Part A: Appl Sci Manuf 2013;46:122–30.

[36] Xu Y, Singh Y, Pan C, Subbarayan G. Adhesive toughness and instability in bonded heterogeneous films. Int J Solids Struct 2019;169:41–54.

[37] Farmand-Ashtiani E, Cugnoni J, Botsis J. Specimen thickness dependence of large scale fiber bridging in mode i interlaminar fracture of carbon epoxy composite. Int J Solids Struct 2015;55:58–65.

[38] Alfano M, Lubineau G, Paulino GH. Global sensitivity analysis in the identification of cohesive models using full-field kinematic data. Int J Solids Struct 2015;55:66–78.

[39] Canal LP, Alfano M, Botsis J. A multi-scale based cohesive zone model for the analysis of thickness scaling effect in fiber bridging. Compos Sci Technol 2017;139:90–8.

[40] Tao R, Li X, Yudhanto A, Alfano M, Lubineau G. On controlling interfacial heterogeneity to trigger bridging in secondary bonded composite joints: An efficient strategy to introduce crack-arrest features. Compos Sci Technol 2020;188:107964–70.

[41] Liu P, Hu Z, Wang S, Liu W. Finite element analysis of the void growth and interface failure of ductile adhesive joints. J Fail Anal Prev 2018;18(2):291–303.

[42] Suzuki T, Matsuzaki R, Todoroki A, Mizutani Y. Crack growth analysis of a composite/adhesive interface toughened by in-mold surface preparation. Int J Adhes Adhes 2013;42:36–43.

[43] Jain S, Liechti KM, Bonnecaze RT. Cohesive zone models to understand the interface mechanics of thin film transfer printing. J Appl Phys 2019;125(7):75301–10.

[44] Wagih A, Tao R, Yudhanto A, Lubineau G. Improving mode II fracture toughness of secondary bonded joints using laser patterning of adherends. Compos Part A: Appl Sci Manuf 2020:105892–8.

[45] Hashemi S, Kinloch AJ, Williams J. The analysis of interlaminar fracture in uniaxial fibre-polymer composites. Proc R Soc Lond A Math Phys Sci 1990;427(1872):173–99.

[46] Kanninen M. A dynamic analysis of unstable crack propagation and arrest in the DCB test specimen. Int J Fract 1974;10(3):415–30.

[47] Williams J. End corrections for orthotropic DCB specimens. Compos Sci Technol 1989;35(4):367–76.

[48] Tao R, Li X, Yudhanto A, Alfano M, Lubineau G. Laser-based interfacial patterning enables toughening of CFRP/epoxy joints through bridging of adhesive ligaments. Compos Part A: Appl Sci Manuf 2020:106094–9.

[49] Haider A-Z, Zhao X-L, Al-Mihaidi R. Mechanical behaviour of normal modulus carbon fibre reinforced polymer (cfrp) and epoxy under impact tensile loads. Procedia Eng 2011;10:2453–8.

[50] Maimí P, Wagih A, Ortega A, Xavier J, Blanco N, Camanho PP. On the experimental determination of the j-curve of quasi-brittle composite materials. Int J Fract 2020;224(2):199–215.

[51] Daghia F, Cluzel C. The climbing drum peel test: An alternative to the double cantilever beam for the determination of fracture toughness of monolithic laminates. Compos Part A: Appl Sci Manuf 2015;78:70–83.

[52] Maimí P, Turon A, Trias D. Crack propagation in quasi-brittle two-dimensional isotropic lattices. Eng Fract Mech 2011;78(1):60–70.

[53] Marami G, Nazari SA, Faghidian SA, Vakili-Tahami F, Etemadi S. Improving the mechanical behavior of the adhesively bonded joints using RGO additive. Int J Adhes Adhes 2016;70:277–86.

[54] Khoramishad H, Ebrahimijamal M, Fasihi M. The effect of graphene oxide nano-platelets on fracture behavior of adhesively bonded joints. Fatigue Fract Eng Mater Struct 2017;40(11):1905–16.

[55] Maloney K, Fleck N. Toughening strategies in adhesive joints. Int J Solids Struct 2019;158:66–75.

[56] Yudhanto A, Almulhim M, Kamal F, Tao R, Fatta L, Alfano M, Lubineau G. Enhancement of fracture toughness in secondary bonded CFRP using hybrid thermoplastic/thermoset bondline architecture. Compos Sci Technol 2020;199:108346.

[57] Quan D, Murphy N, Ivankovic A. Fracture behaviour of epoxy adhesive joints modified with core-shell rubber nanoparticles. Eng Fract Mech 2017;182:566–76.

[58] Wagih A, Lubineau G. Enhanced mode II fracture toughness of secondary bonded joints using tailored sacrificial cracks inside the adhesive. Compos Sci Technol 2021;204:108605.

[59] Bao G, Suo Z. Remarks on crack-bridging concepts. Appl Mech Rev 1992;45:355–66.